An inertial human upper limb motion tracking method for robot programming by demonstration

Robin Pellois, Olivier Brüls

Department of Aerospace and Mechanical Engineering, University of Liège

robin.pellois@uliege.be, o.bruls@uliege.be

Abstract

This paper proposes an inertial human motion tracking for robot programming by demonstration (PbD). An original element called heading reset is proposed to catch the drift around gravity direction. It is based on a hypothesis made on the human arm motion during a task demonstration. It is used to overcome the non-use of the magnetometer due to magnetic disturbances from robotic environment. This element is implemented in an orientation estimation algorithm and compared with three other IMU algorithms and a commercial MARG algorithm. The human arm trajectory is estimated through three IMUs sensors directly set on the arm to estimate the segment orientation (hand, forearm and arm). A specific inertial-2-segment procedure is presented as well as a procedure to estimate the transformation from human reference frame to task frame, necessary for a PbD process. Experimental tests, using a robot as a reference, have been conducted to validate the different part of the method. The heading reset and the orientation algorithm show good results. The inertial-2-segment procedure is shown to be robust. Finally, experimental tests on a human arm and physical robot validate the complete method.

Keywords: Robotics; Programming by demonstration; Inertial human motion tracking

1. Introduction

Programming by demonstration (PbD) [1] is a paradigm that aims at teaching tasks to a robot through human demonstrations. Inspired by the way human interact, it makes robot programming easier and more accessible in an industrial context as well as in

daily life [2]. A PbD process has two steps: gathering a dataset from the teacher demonstration and deriving a policy from the dataset. The problem of deriving a policy is decomposed into 4 questions: What to imitate? How to imitate? When to imitate? Whom to imitate? Up to date, most papers in the literature focused on the first 2 questions. The first question addresses the extraction of the tasks features from the dataset. The second question addresses to the ability of the robot to adapt to new configurations of the task. This work focus on the first step of the PbD process: gathering a dataset. A dataset is constituted of data recorded during the demonstrations made by the teacher. Each recording of a demonstration can be seen as a set of states Z_t and actions A_t representing the task demonstrated by the teacher. According to Argal et al. [3], "for [PbD] to be successful, the states and actions in the learning dataset must be usable by the [learner]". The learner needs therefore a set of states Z_l and actions A_l that represent the demonstrated task in a meaningful way for him. The process of gathering dataset, or recording demonstrations, faces then the correspondence issue, i.e., the identification of mappings between $[Z_t;A_t]$ and $[Z_l;A_l]$.

According to [3], two mappings may be necessary regarding the demonstration technique: a record mapping and/or an embodiment mapping. If the human states and actions during the demonstration are not directly recorded, a record mapping is necessary. Then, if the dataset recorded is not executable by the robot, an embodiment mapping is necessary. For instance, if the human motion is recorded by cameras, extracting human motion from images constitutes a record mapping. If the human motion is expressed as joint angles and if the human and the robot do not have the same kinematics, an embodiment mapping is necessary. Regarding the necessary mapping functions, 4 categories of demonstrations can be made: teleoperation, shadowing, sensors-on-instructor and external-observation. In the teleoperation category, which gathers method such as kynesthesy, the robot executes the demonstration guided or operated by the human [4, 5, 6]. In such cases, the correspondence problem is trivial since the demonstration is recorded from the robot own encoders and sensors, making kinesthesy one of the most largely used methods. However, these methods prevent natural human motion which reduces the range of applications. For instance, a painting task [7], requiring dexterity, could hardly be achieved this way. In shadowing, the

robot mimics the teacher and record its own motion, therefore only record mapping is necessary [8, 9]. In the sensors-on-instructor category, the human demonstrations are recorded through an external device that records directly the variables of interest so that, only embodiment mapping is required [10, 11, 12]. Finally, the last category requires both record and embodiment mapping. In [7], a marker-based vision tracking device measured the trajectory of a painting tool. In [13], a six wheel-legged robot [14] follows a generalized trajectory over human trajectory observations with a single Kinect camera. The Kinect sensor tracks the human teacher through the extraction of skeleton points. In [15], a Dynamic Vision Sensor tracks human hand changes of state to learn different movements from a single demonstration depending on visual cues. This category gathers user-friendly demonstration methods but suffers from difficulties to identify mapping functions. Recording demonstration methods requires a compromise between the difficulty of identifying mapping functions and the convenience for the teacher to use.

Humans use a large panel of communication channels and a privileged one is gestures. Human gestures and arm motions in particular are largely used in human-human interactions as shown in [16] and [17]. Furthermore, programming a robot consists mainly in commanding the position of its gripper. The correspondence with the human hand is immediate, so it is considered that one of the main variables of interest in a demonstration of a task is the human hand trajectory and state. However, this trajectory with respect to the teacher frame is not relevant for the learner. In order for the demonstrated task to be reproduced by the learner, the recorded elements have to be expressed with respect to a frame that is meaningful for the learner: the task frame. Identifying transformations to the task frame is part of the embodiment mapping. Let us keep in mind that for some tasks that involve, for instance, manipulated object [2, 18, 19, 10], tools [20], etc.; other elements should be recorded during the demonstrations with respect to the task frame.

The objective of this work is then to develop a method to estimate the human hand trajectory with respect to the task frame in the context of robot PbD. The method should satisfy the constraints from PbD: easiness of use and no hindering of human gestures.

An appropriate human motion capture technology is therefore necessary. Field et

al., [21] expose a survey of human motion capture methods in robotics. Cameras and optoelectronics systems have the advantage of giving the position in a well-known reference frame. But such devices face concealment problems due to environment (light, dust, smokes) or movement of the operator. Mechanical devices such as exoskeletons measure the relative motion of human joints directly which can be easily mapped to a human body model but does not directly give the absolute trajectory with respect to a fixed reference frame. Exoskeletons may also be heavy, intrusive and uncomfortable for the operator and could also limit operator motion by the mechanical constraints of the structure. Devices based on the measurement of a known magnetic field are mentioned but are not appropriate in an industrial environment due to their high sensitivity to magnetic disturbances. Alternatively, Inertial Measurement Units (IMUs) [22, 23] are small, light and cheap (for the MEMS version) making them suitable for wearable devices, even embedded in clothes [24] and do not require the use of external apparatus such as cameras. However, IMU data require complex treatment and signal filtering in the trajectory reconstruction process. Each technology has its own advantages and drawbacks making them more or less suitable depending on the context of the application. Regarding the practicality of the system, opto-electronic and mechanical devices seem more cumbersome than IMUs. IMUs can thus better meet the expected intuitiveness and easiness of use in PbD. However, challenges appear when using inertial sensors for human motion tracking (IHMT), especially in a robotic environment. IMUs are not measuring directly the trajectory of the hand, therefore, a record mapping is necessary.

Only a few solutions can be mentioned regarding IHMT for PbD. Human joint angles are recorded in [25] with an inertial suit to teach primitive motion to a humanoid robot. In [26], a humanoid robot is taught basket referee gestures. The dataset is constituted of human motion recorded through inertial sensors and, in a second step, kinesthetics demonstrations. In [27], IMU is used to counter concealment issues during vision based tool tracking during the teaching of a painting task. The solution proposed in [28] only enables teleoperation of the robot and would fall into the same category as kinesthesy. However, IHMT has been investigated for a wide range of applications including robotics [22, 29]. The lack of inertial-based demonstration acquiring method

in PbD despite a large amount of work in IHMT, motivate this work.

In IHMT, two approaches have been identified as the kinematic chain and the free segment approach [30]. The kinematic chain approach consists of estimating joint angles from measurement of sensors placed before and after the joint in the kinematic chain [31, 32]. The free segment approach consists of estimating the orientation of each segment with respect to an inertial reference frame using the sensor attached to the segment [33, 34]. The two methods could in principle lead to the same information. The free segment approach seems more suitable when the targeted measurement is the hand position and not the joint angle. This approach is combined with a simple human arm kinematic model with spherical joints for the wrist, elbow and shoulder.

One challenge in IHMT is to identify the positioning of the sensors with respect to the human arm (referred in literature as inertial-to-segment (I2S) calibration). Some methods assume that sensors are aligned with the segment; therefore these parameters do not need to be evaluated [35, 36]. Other techniques rely on static positions (e.g., N-pose, T-pose) [37, 38, 39] or on complex functional motion [40, 41].

In order to be meaningful to the robot, it is necessary to localize the human and the robot with respect to the task frame. Different approaches have been studied in the literature, based on external or embedded extra sensors [42, 43], markers [44], or a specific procedure [45]. The use of extra sensors does not seem suitable to keep the workability of the method for PbD. Considering the task frame as the robot frame, a simple procedure is proposed to estimate this transformation. It is based on a least square method applied on recorded data from trajectory imposed to the teacher by the robot. This step in the method corresponds to the embodiment mapping.

Contribution: this work proposes an IHMT method to express human hand trajectory with respect to the task/robot frame, and which fulfills the requirements of a PbD process. Within this IHMT method, a new I2S procedure is proposed consisting of one functional motion followed by a static pose as well as a procedure to express human hand trajectory with respect to the robot frame. We also propose to take advantage of the robot to add an extra step consisting in optimizing some parameters of the IHMT method.

In our method as in most of IHMT method, the IMUs orientation estimation is re-

quired. The main challenge related to this sensor is to manage the drift from gyroscope data integration as explained in [22], for instance. One very documented approach couples an IMU with a magnetometer (MARG or MIMU sensor) to measure the Earth north direction. However, the magnetometer signal is easily disturbed [46, 47, 48], especially in a robotic environment such as PbD. Other works couple IMU with other sensors such as UWB devices in [49]. However, adding extra sensors may decrease the easiness of implementation targeted in our work. Pure IMU orientation usually catches up the gyroscope drift only along direction perpendicular to gravity. Several methods have been explored [50, 51]: complementary filters [52, 53, 54]; Kalman and Extended Kalman filters [55, 56, 57], gradient descent filters [58] or integration and vector observation [59, 60].

Contribution: this work proposes a new approach called heading reset to reduce drift around gravity direction. The heading of a sensor is the part of its orientation around the gravity direction. The heading reset relies on a hypothesis made on human motion in a context of teaching task. In this specific context, it is assumed that the initial configuration of the human arm is such that the hand occupies a central pose in the workspace. In a first-person vision study, a camera is set on the head of the human who has to perform a task in front of him. In [61], Bandini, et al. state that "hands and manipulated objects tend to appear at the center of the image". Furthermore, this position is also centrally located in the workspace of the human arm as discussed in [62, 63]. This indicates that the position of the human hand in front of the subject is a privileged position which is frequently visited during a manipulation task. We assume that the operator initiates the motion around this privileged position, and that the corresponding heading angle also represents a privileged orientation which will be frequently visited during the task. At this moment, a reset of the heading of the sensor is applied. It is not a standalone element, it is implemented at the angular velocity level of an integration and vector observation algorithm.

In this paper, section 2 describes the complete method to estimate the human hand trajectory with respect to the task frame. The algorithm for orientation estimation, the IHMT method and the optimization process are presented. Section 3 presents the tests conducted to validate the different steps of the method. Firstly, the orientation esti-

mation algorithm is compared with other IMU algorithms in a robotics environment. Secondly, the robustness of the initialization procedure is analyzed. Finally, the complete method is evaluated thanks to a Sawyer robot. The robot performs several 3D trajectories while the fingertip of the operator is in contact with the robot end-effector. Therefore, the trajectory estimated by the proposed method can be compared to the trajectory recorded by robot encoders.

2. Human arm motion measurement with IMUs

2.1. Proposed algorithm for IMU orientation estimation

This section describes the method to estimate sensor orientation. First, the integration and vector observation algorithm is presented and then the heading reset method.

Integration and vector observation algorithm.. A sensor frame S is used to describe the sensor motion. At time step 0, the sensor frame is designated by $S0$ and defines the inertial reference frame for the orientation of the sensor. The sensor is considered motionless at this time step. The algorithm also makes use of the sensor frame at time step $n-1$: $S-1$ and at time step n: S. The unit quaternion ${}^{S0}\hat{q}_S$ denotes the rotation from frame S to frame $S0$ and ${}^{S}\hat{q}_{S0} = ({}^{S0}\hat{q}_S)^{-1}$. The cross product is noted $\times$ and the quaternion product $\otimes$. A three-dimensional vector $\mathbf{u}$ can be expressed as a quaternion $\hat{u}$ with no real part but only a vector part $\mathbf{u}$:

$$\hat{u} = \begin{bmatrix} 0 \\ \mathbf{u} \end{bmatrix} = \begin{pmatrix} 0 \\ u_x \\ u_y \\ u_z \end{pmatrix} \tag{1}$$

An IMU sensor measures the angular velocity ${}^{S}\boldsymbol{\omega}^{\text{gyro}}(t)$ and the acceleration ${}^{S}\mathbf{a}(t)$ of the sensor in the frame S. In this work, the model of the gyroscope data is ${}^{S}\boldsymbol{\omega}^{\text{gyro}}(t) = {}^{S}\boldsymbol{\omega}^{\text{true}}(t) + {}^{S}\boldsymbol{\beta}(t) + {}^{S}\boldsymbol{\gamma}(t)$ with ${}^{S}\boldsymbol{\omega}^{\text{true}}(t)$ the true angular velocity of the sensor, ${}^{S}\boldsymbol{\beta}(t)$ a bias and ${}^{S}\boldsymbol{\gamma}(t)$ a noise. The model of the accelerometer data consists of a gravity component ${}^{S}\mathbf{g}(t)$, a linear acceleration component ${}^{S}\mathbf{l}(t)$ and a noise ${}^{S}\mathbf{n}(t)$: ${}^{S}\mathbf{a}(t) = {}^{S}\mathbf{l}(t) + {}^{S}\mathbf{g}(t) + {}^{S}\mathbf{n}(t)$. IMUs data needs to be filtered to manage noise and calibrated (to

determine bias, misalignment and gain/sensitivity). Solutions have been proposed as in [64, 65]. However, this question is not the purpose of this work and it is assumed that the sensor data have been pre-filtered and are reliable. Only a moving window average is applied at the end of the method to smooth the trajectory. The kinematic equation of a rigid body describes the variation of its orientation as:

$$\dot{\hat{q}} = \frac{1}{2}\hat{q} \otimes {}^{S}\hat{\omega}(t) \tag{2}$$

The above equation is solved with the explicit Euler method on the Lie group of quaternion [66]

$${}^{S0}\hat{q}_S = {}^{S0}\hat{q}_{S-1} \otimes \exp(\frac{1}{2}\Delta t \ {}^{S}\hat{\omega}_n) \tag{3}$$

with Δt the time step value and ${}^{S}\hat{\omega}_n$ the estimated angular velocity at time step n in the frame S and the exponential map

$$\exp(\hat{u}) = \begin{pmatrix} \cos(\|\mathbf{u}\|) \\ \sin(\|\mathbf{u}\|)\frac{u_x}{\|\mathbf{u}\|} \\ \sin(\|\mathbf{u}\|)\frac{u_y}{\|\mathbf{u}\|} \\ \sin(\|\mathbf{u}\|)\frac{u_z}{\|\mathbf{u}\|} \end{pmatrix} \tag{4}$$

The integration of the gyroscope measurement ${}^{S}\boldsymbol{\omega}_n^{\text{gyro}}$ using this algorithm leads to a drift of the orientation due to the gyroscope bias ${}^{S}\boldsymbol{\beta}$. The gravity vector estimation from accelerometer measurement enables to partly compensate the drift in phases when the sensor is almost stationary. A moment is considered stationary if ${}^{S}l \approx 0$, which implies that $\frac{{}^{S}a}{\|{}^{S}a\|} \approx {}^{S}g$. Let us introduce the geometric vector $\mathbf{d}$, a unit vector which follows the motion of the sensor (see Fig. 1). This vector is defined as aligned with the gravity vector at time step $n-1$, i.e., in the frame $S-1$, we have ${}^{S-1}\mathbf{d}_{n-1} = {}^{S-1}\mathbf{g}$. Also the same vector $\mathbf{d}$ at time step $n-1$ but projected in the frame S satisfies ${}^{S}\mathbf{d}_{n-1} = {}^{S}\mathbf{g}$. The vector $\mathbf{d}$ being constant with respect to the sensor frame, the projection of $\mathbf{d}$ at time step $n-1$ in the sensor frame $S-1$ is equal to the projection of $\mathbf{d}$ at time step n in sensor frame S, ${}^{S}\mathbf{d}_n = {}^{S-1}\mathbf{d}_{n-1} = {}^{S-1}\mathbf{g}$. The rotation ${}^{S-1}\hat{q}_S$ can be decomposed as ${}^{S-1}\hat{q}_S = {}^{S-1}\hat{q}_* \otimes {}^{*}\hat{q}_S$. The rotation ${}^{*}\hat{q}_S$ is defined as the rotation about an axis perpendicular to the plane containing the vectors ${}^{S}\mathbf{d}_n$ and ${}^{S}\mathbf{d}_{n-1}$ which rotates the vector ${}^{S}\mathbf{d}_{n-1}$ to

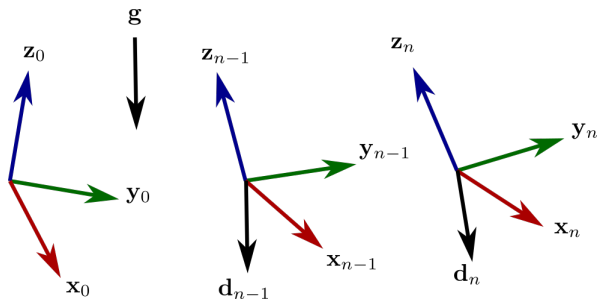

Figure 1: definition of the vector $\mathbf{d}$

${}^{S}\mathbf{d}_n$. The rotation angle of ${}^{*}\hat{q}_S$ being small when the sensor is almost stationary, its rotation vector is estimated as ${}^{S}\mathbf{d}_{n-1} \times {}^{S}\mathbf{d}_n$, which is equal to ${}^{S}\mathbf{g} \times {}^{S-1}\mathbf{g}$. The rotation ${}^{S-1}\hat{q}_*$ is a rotation about an axis aligned with ${}^{S}\mathbf{d}_{n-1} = {}^{S}\mathbf{g}$ and it can be estimated by the integration of the projection of the gyroscope measurement on ${}^{S}\mathbf{g}$. Thereby, a modified angular velocity ${}^{S}\boldsymbol{\omega}_n^{\text{mod}}$ is computed as

$$ {}^{S}\boldsymbol{\omega}_n^{\text{mod}} = \frac{1}{\Delta t}({}^{S}\mathbf{g} \times {}^{S-1}\mathbf{g}) + (I_3 + {}^{S}\tilde{\mathbf{g}}\,{}^{S}\tilde{\mathbf{g}})\,{}^{S}\boldsymbol{\omega}_n^{\text{gyro}} \tag{5} $$

with I_3 is the identity matrix of dimension 3 and $\tilde{\mathbf{u}}$ represents the skew-symmetric matrix defined from the vector $\mathbf{u}$ as

$$ \begin{pmatrix} 0 & -u_z & u_y \\ u_z & 0 & -u_x \\ -u_y & u_x & 0 \end{pmatrix}. $$

Figure 2 illustrates the different components of ${}^{S}\boldsymbol{\omega}_n^{\text{mod}}$. A key point of the proposed algorithm is to evaluate ${}^{S-1}\mathbf{g}$ using the estimated rotation at time $n-1$ according to ${}^{S-1}\hat{g} = {}^{S-1}\hat{q}_{S0} \otimes {}^{S0}\hat{g} \otimes {}^{S0}\hat{q}_{S-1}$, where ${}^{S0}\mathbf{g}$ is the gravity measured in the initial configuration of the sensor. Indeed, the sensor being motionless at time step 0, the linear acceleration is negligible ${}^{S0}\mathbf{l} \approx 0$ and ${}^{S0}\mathbf{g} \approx \frac{{}^{S0}\mathbf{a}_0}{\|{}^{S0}\mathbf{a}_0\|}$. This evaluation of ${}^{S-1}\mathbf{g}$ is thus affected by the drift of the estimated rotation. In contrast, ${}^{S}\mathbf{g}$ is evaluated by direct estimation from the accelerometer signal as ${}^{S}\mathbf{l} \approx 0$ and ${}^{S}\mathbf{g} \approx \frac{{}^{S}\mathbf{a}_n}{\|{}^{S}\mathbf{a}_n\|}$, which is valid when the sensor is stationary. The evaluation of ${}^{S}\mathbf{g}$ is thus free from any drift. In this way, the algorithm will automatically compensate the accumulated rotation drift captured

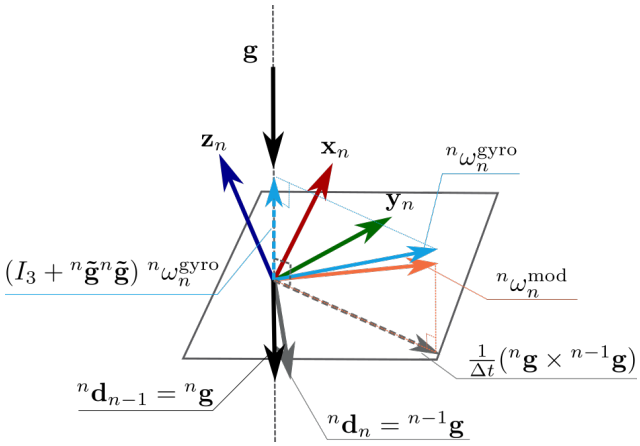

Figure 2: Components of ${}^S\boldsymbol{\omega}_n^{\text{mod}}$

by the operation ${}^S\mathbf{g} \times^{S-1} \mathbf{g}$. The component of ${}^S\boldsymbol{\omega}_n^{\text{mod}}$ along the gravity direction is still obtained from the gyroscope measurement and the drift along this direction is not compensated. To identify stationary periods, as advised in [53], the norm of the accelerometer measurement is compared to the gravity acceleration g according to the criterion $|\|{}^S\mathbf{a}_n\| - g| < k_a$ with the threshold k_a tuned to $k_a = 0.1$ g-unit. However, our experience is that this criterion is not sufficiently restrictive in the sense that it can be fulfilled even if $\frac{{}^S\mathbf{a}_n}{\|{}^S\mathbf{a}_n\|}$ differs from ${}^S\mathbf{g}$. Having a good approximation of ${}^S\mathbf{g}$ is essential and motivates a more restrictive criterion for stationary periods detection. During a stationary period, $\frac{{}^S\mathbf{a}_n}{\|{}^S\mathbf{a}_n\|} \approx {}^S\mathbf{g}$ implies $\frac{{}^{S0}\mathbf{a}_n}{\|{}^{S0}\mathbf{a}_n\|} \approx {}^{S0}\mathbf{g}$. By definition, $\frac{d({}^{S0}\mathbf{g})}{dt} = 0$, so we expect $\frac{d({}^{S0}\mathbf{a})}{dt} = 0$, which leads to the criterion $\|\frac{{}^{S0}\mathbf{a}_n - {}^{S0}\mathbf{a}_{n-1}}{\Delta t}\| < k_d$ with the additional threshold $k_d = 1$ g-unit.s^{-1}. The acceleration with respect to the inertial frame $S0$ is computed as

$$ {}^{S0}\hat{a}_{n-1} = {}^{S0}\hat{q}_{S-1} \otimes {}^{S-1}\hat{a}_{n-1} \otimes {}^{S-1}\hat{q}_{S0} \tag{6} $$

$$ {}^{S0}\hat{a}_n = {}^{S0}\hat{q}'_S \otimes {}^{S}\hat{a}_n \otimes {}^{S}\hat{q}'_{S0} \tag{7} $$

where ${}^{S0}\hat{q}'_S$ is an estimation the orientation of the sensor based on the gyroscope signal:

$$ {}^{S0}\hat{q}'_S = {}^{S0}\hat{q}_{S-1} \otimes \exp(\frac{1}{2}\Delta t\ {}^S\hat{\omega}_n^{\text{gyro}}) \tag{8} $$

To the best of our knowledge, such a criterion has not been proposed yet. The threshold

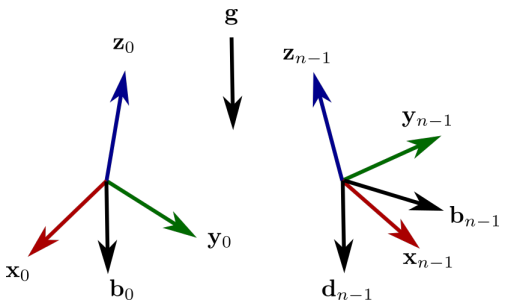

Figure 3: definition of the vector **b**

values have been adjusted by trial-and-error on experimental data.

Heading reset. An additional original method, called heading reset, to compensate the drift along the gravity direction is proposed. The heading, which will be formally defined below, represents the part of the sensor orientation along the gravity direction. The original heading is the heading at time step 0, which is the identity. It is expected that the operator executes left-right motion such that the sensor pass by its original heading. This is exploited to reset the drift around the gravity direction each time this situation is encountered. If the application does not involve heading reset, the orientation estimation will have the accuracy of the basic algorithm. The heading reset is applied through a correction ${}^{S}\boldsymbol{\omega}_n^{\text{reset}}$ at the angular velocity level. The total rotation ${}^{S0}\hat{q}_{n-1}$ can be decomposed into an inclination and a heading part as ${}^{S0}\hat{q}_{n-1} = {}^{S0}\hat{q}_{*} \otimes {}^{*}\hat{q}_{n-1}$. The rotation axis of the heading part ${}^{*}\hat{q}_{n-1}$ is the gravity vector, so ${}^{S-1}\mathbf{g} = {}^{*}\mathbf{g}$. Similarly to the vector **d**, a vector **b** is defined as a vector constant for an observer following the sensor frame and aligned with the gravity vector at time step 0: ${}^{S0}\mathbf{b}_0 = {}^{S0}\mathbf{g} = {}^{S-1}\mathbf{b}_{n-1}$ (see Fig. 3). The rotation ${}^{*}\hat{q}_0$ is the inclination part and its rotation axis ${}^{*}\boldsymbol{\theta}_0$ is computed as ${}^{*}\boldsymbol{\theta}_0 = \frac{{}^{S0}\mathbf{g} \times {}^{S-1}\mathbf{g}}{\|{}^{S0}\mathbf{g} \times {}^{S-1}\mathbf{g}\|} \text{asin}(\|{}^{S0}\mathbf{g} \times {}^{S-1}\mathbf{g}\|)$. Therefore ${}^{*}\hat{q}_0$ is computed as ${}^{*}\hat{q}_0 = \exp({}^{*}\boldsymbol{\theta}_0)$. Then ${}^{S}\boldsymbol{\omega}_n^{\text{reset}}$ is computed as

$$ {}^{*}\hat{q}_{n-1} = {}^{*}\hat{q}_0 \otimes {}^{S0}\hat{q}_{n-1} \tag{9} $$

$$ {}^{S}\boldsymbol{\omega}_n^{\text{reset}} = \frac{1}{\Delta t} \log({}^{*}\hat{q}_{n-1}) \tag{10} $$

with the logarithm map $\log(\hat{q})$

$$\log(\hat{q}) = \frac{2\,\mathrm{acos}(\hat{q}_1)}{\sqrt{\hat{q}_2^2+\hat{q}_3^2+\hat{q}_4^2}} \begin{pmatrix} \hat{q}_2 \\ \hat{q}_3 \\ \hat{q}_4 \end{pmatrix} \tag{11}$$

and subtracted to the angular velocity. The sensor is considered close to its initial heading when $\|\Delta t\ {}^{S}\boldsymbol{\omega}_n^{\text{reset}}\| < k_r$. A too low value of the tolerance k_r will not catch the drift and a too high value will annihilate any rotation around the gravity direction. The value of this tolerance is tuned at 0.1 rad meaning that the sensor is considered close to its original heading when the estimated heading is under 0.1 rad. In order to limit overly heading reset, the corrective term is applied only when the sensor is stationary. This extra condition to apply the reset is necessary. Without any restriction, the reset may be applied to each iteration annihilating any rotation around the gravity direction. Applying the reset only when the sensor is stationary enables to catch up the accumulated error from gyroscope data integration but not the heading component of the sensor orientation. The complete orientation estimation process is detailed in algorithm 1.

Algorithm 1 : Complete IMU orientation algorithm

$^{S0}\hat{a}_{n-1} = {}^{S0}\hat{q}_{S-1} \otimes {}^{S-1}\hat{a}_{n-1} \otimes {}^{S-1}\hat{q}_{S0}$

$^{S0}\hat{q'}_S = {}^{S0}\hat{q}_{S-1} \otimes \exp(\frac{1}{2}\Delta t \; {}^{S}\hat{\omega}_n^{\text{gyro}})$

$^{S0}\hat{a}_n = {}^{S0}\hat{q}_S \otimes {}^{S}\hat{a}_n \otimes {}^{S}\hat{q}_{S0}$

if $|\|{}^{S}\mathbf{a}_n\| - g| < k_a$ **and** $\|\frac{{}^{S0}\mathbf{a}_n - {}^{S0}\mathbf{a}_{n-1}}{\Delta t}\| < k_d$ **then**

  $^{S0}\mathbf{g} = \frac{{}^{S0}\mathbf{a}_0}{\|{}^{S0}\mathbf{a}_0\|}$

  $^{S}\mathbf{g} = \frac{{}^{S}\mathbf{a}_n}{\|{}^{S}\mathbf{a}_n\|}$

  $^{S-1}\hat{g} = {}^{S-1}\hat{q}_{S0} \otimes {}^{S0}\hat{g} \otimes {}^{S0}q_{S-1}$

  $^{S}\boldsymbol{\omega}_n^{\text{mod}} = \frac{1}{\Delta t}({}^{S}\mathbf{g} \times {}^{S-1}\mathbf{g}) + (I_3 + {}^{S}\tilde{\mathbf{g}}\,{}^{S}\tilde{\mathbf{g}})\,{}^{S}\boldsymbol{\omega}_n^{\text{gyro}}$

  $^{*}\boldsymbol{\theta}_{S0} = \frac{{}^{S0}\mathbf{g} \times {}^{S-1}\mathbf{g}}{\|{}^{S0}\mathbf{g} \times {}^{S-1}\mathbf{g}\|} \operatorname{asin}(\|{}^{S0}\mathbf{g} \times {}^{S-1}\mathbf{g}\|)$

  $^{*}\hat{q}_{S-1} = \exp({}^{*}\hat{\theta}_{S0}) \otimes {}^{S0}\hat{q}_{S-1}$

  $^{S}\boldsymbol{\omega}_n^{\text{reset}} = \frac{1}{\Delta t}\log({}^{*}\hat{q}_{S-1})$

  if $\|\Delta t \; {}^{S}\boldsymbol{\omega}_n^{\text{reset}}\| < k_r$ **then**

    $^{S}\boldsymbol{\omega}_n = {}^{S}\boldsymbol{\omega}_n^{\text{mod}} - {}^{S}\boldsymbol{\omega}_n^{\text{reset}}$

  else

    $^{S}\boldsymbol{\omega}_n = {}^{S}\boldsymbol{\omega}_n^{\text{mod}}$

  end if

else

  $^{S}\boldsymbol{\omega}_n = {}^{S}\boldsymbol{\omega}_n^{\text{gyro}}$

end if

$^{S0}\hat{q}_S = {}^{S0}\hat{q}_{S-1} \otimes \exp(\frac{1}{2}\Delta t \; {}^{S}\hat{\omega}_n)$

2.2. Hand trajectory estimation

This section describes the method to estimate the hand trajectory with respect to the task frame from sensor orientation estimation.

190 *System description.* In order to track segment orientation, one sensor is fastened on each arm segment with an arbitrary position and orientation. The hand is considered as a single rigid segment, i.e., no finger motion is measured. The torso is considered motionless. The frames attached to the sensors, at time step n, are noted $S1n$, $S2n$ and $S3n$, respectively for the segment 1 for the arm, 2 for the forearm and 3 for the hand

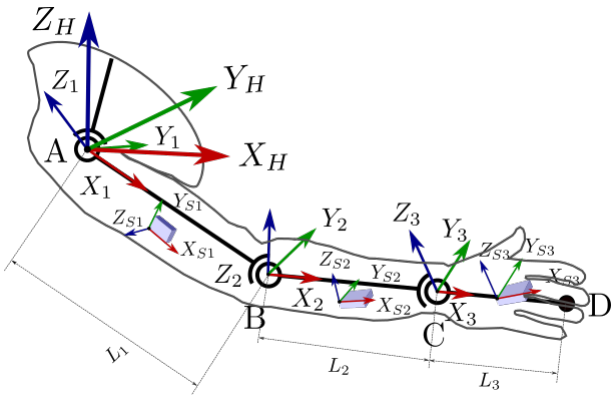

Figure 4: Human arm model

(see Fig. 4). The initial sensor frames are therefore respectively noted $S10$, $S20$, $S30$.

Human arm model. The kinematic model of the human arm used in this work is composed of 3 spherical joints for the shoulder, elbow and wrist as described in Figure 4. The human attached inertial frame noted H is centered on the shoulder joint, its $\boldsymbol{z}$-axis is along the gravity and pointing upwards and its $\boldsymbol{x}$-axis, parallel to the sagittal plane, is decribed later. Frames $1n$, $2n$ and $3n$ respectively denote the frames attached to the segments 1, 2 and 3 and centered at the joint at time step n. Their $\boldsymbol{x}$-axes are aligned with the direction of the segment and pointing towards the next joint center in the chain. L_1, L_2 and L_3 are the segment lengths. L_3 is defined as the distance from the finger tip D to the middle point between the radial styloid and the ulnar styloid. L_2 is defined as the distance from the middle point between the radial styloid and the ulnar styloid to the middle point between the lateral and the medial epicondyle. L_1 is defined as the distance from the middle point between the lateral and the medial epicondyle to the tip of the acromion bone.

Hand trajectory. The vector ${}^{H}\mathbf{AD}_n$ represents the position of the hand with respect to the frame H at time step n and can be evaluated from the orientation of the segments 1, 2 and 3 as

$$ {}^{H}\hat{AD}_n = {}^{H}\hat{AB}_n + {}^{H}\hat{BC}_n + {}^{H}\hat{CD}_n \tag{12} $$

with

$$^{H}\hat{AB}_n = {}^{H}\hat{q}_{1n} \otimes {}^{1n}\hat{AB}_n \otimes {}^{1n}\hat{q}_H \tag{13}$$

$$^{H}\hat{BC}_n = {}^{H}\hat{q}_{2n} \otimes {}^{2n}\hat{BC}_n \otimes {}^{2n}\hat{q}_H \tag{14}$$

$$^{H}\hat{CD}_n = {}^{H}\hat{q}_{3n} \otimes {}^{3n}\hat{CD}_n \otimes {}^{3n}\hat{q}_H \tag{15}$$

with ${}^{1n}\mathbf{AB}_n = [L_1\ 0\ 0]^T$, ${}^{2n}\mathbf{BC}_n = [L_2\ 0\ 0]^T$, ${}^{3n}\mathbf{CD}_n = [L_3\ 0\ 0]^T\ \ \forall n$. The rotation ${}^{H}\hat{q}_{in}$ can be decomposed as

$$^{H}\hat{q}_{in} = {}^{H}\hat{q}_{Si0} \otimes {}^{Si0}\hat{q}_{Sin} \otimes {}^{Sin}\hat{q}_{in} \tag{16}$$

Algorithm 1 gives an estimation of ${}^{Si0}\hat{q}_{Sin}$ based on IMU measurements. The I2S (inertial-to-segment) orientation of the sensor with respect to the segment ${}^{in}\hat{q}_{Sin}$ and the initial orientation of the sensor with respect to the human frame ${}^{H}\hat{q}_{Si0}$ are estimated through an initialization procedure.

Initialization procedure. Assuming that the motion of the skins and soft tissues can be neglected, the I2S orientation is constant, i.e.,

$$^{Sin}\hat{q}_{in} = {}^{Si0}\hat{q}_{i0}\ \ \forall n. \tag{17}$$

It is asked to the operator to start the trajectory with the arm horizontal, outstretched and in the sagittal plane as illustrated in Figure 5 a. In this configuration, the segment frame $i0$ is aligned with the inertial human reference frame H, i.e.,

$$^{Si0}\hat{q}_{i0} = {}^{Si0}\hat{q}_{H}. \tag{18}$$

The $\mathbf{z}$-axis of the reference frame H being along the gravity direction, it is estimated through accelerometer measurement when the operator is at the initial position. Previously, the operator performs a shoulder flexion in the sagittal plane (see Fig. 5 b), so that the $\boldsymbol{y}$-axis of the reference frame H can be defined as the normalized projection of the angular velocity in the plane perpendicular to $\boldsymbol{z}$-axis. In this way, the transformation ${}^{Si0}\hat{q}_{H}$ is obtained for each sensor i. Table 1 details the initialization procedure related to segment i.

1	Rotation around the shoulder-shoulder axis with a straight arm	N recording of $\boldsymbol{\omega}_k$
2	Computation of $\mathbf{y}_\omega$	$\mathbf{y}_\omega = \frac{1}{N} \sum_{k=1}^{N} \frac{\boldsymbol{\omega}_k}{\|\boldsymbol{\omega}_k\|}$
3	Arm locked in initial position	N recording of $\mathbf{a}_k$
4	Computation of ${}^{Si0}\mathbf{z}_H$	${}^{Si0}\mathbf{z}_H = -\frac{1}{N} \sum_{k=1}^{N} \frac{\mathbf{a}_k}{\|\mathbf{a}_k\|}$
5	Projection of $\mathbf{y}_\omega$	$\mathbf{y}'_\omega = -(\mathbf{y}_\omega - (\mathbf{y}_\omega \cdot {}^{Si0}\mathbf{z}_H){}^{Si0}\mathbf{z}_H)$
6	Computation of ${}^{Si0}\mathbf{y}_H$	${}^{Si0}\mathbf{y}_H = \frac{\mathbf{y}'_\omega}{\|\mathbf{y}'_\omega\|}$
7	Computation of ${}^{Si0}\mathbf{x}_H$	${}^{Si0}\mathbf{x}_H = {}^{Si0}\mathbf{y}_H \times {}^{Si0}\mathbf{z}_H$
8	Computing of rotation matrix	${}^{Si0}R_H = \left[{}^{Si0}\mathbf{x}_H {}^{Si0}\mathbf{y}_H {}^{Si0}\mathbf{z}_H\right]$
9	Conversion to quaternion	${}^{Si0}R_H \rightarrow {}^{Si0}\hat{q}_H$
10	Computation of ${}^{H}\hat{q}_{Si0}$ and ${}^{Sin}\hat{q}_{in}$	${}^{H}\hat{q}_{Si0} = ({}^{Si0}\hat{q}_H)^{-1}$; ${}^{Sin}\hat{q}_{in} = {}^{Si0}\hat{q}_H$

Table 1: Steps of the initialization of the human arm measurement process

Human-robot transformation estimation. It is considered in our work that the task frame is the robot base frame. The embodiment mapping consists then in the estimation of the transformation from the human inertial reference frame H with origin A to the robot based frame R with origin O, composed of a rotation part ${}^{R}\hat{q}_H$ and a translation part ${}^{R}\mathbf{AO}$. Once the initialization procedure is finished, the operator puts its fingertip in contact with the robot end-effector and follows an arbitrary trajectory imposed by the robot. During the trajectory, N human fingertip positions ${}^{H}\mathbf{AD}_k$ and robot end-effector

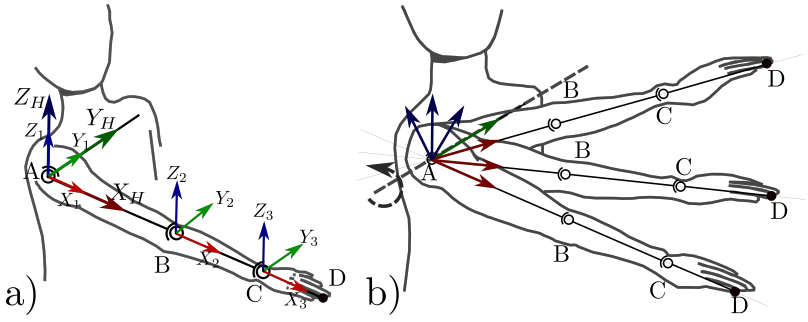

Figure 5: a) Initial position ; b) Rotation around shoulder-shoulder axis

positions ${}^{R}\mathbf{P}_k$ are recorded. The rotation ${}^{R}\hat{q}_H$ is estimated using a least square method [67]. The first step is to compute the centroid of each data set ${}^{H}\mathbf{AD}$ and ${}^{R}\mathbf{P}$ as

$$ {}^{H}\mathbf{AD} = \frac{1}{N}\sum_{k=1}^{N} {}^{H}\mathbf{AD}_k \tag{19} $$

$$ {}^{R}\mathbf{P} = \frac{1}{N}\sum_{k=1}^{N} {}^{R}\mathbf{P}_k. \tag{20} $$

The rotational matrix Q corresponding to ${}^{R}\hat{q}_H$ is estimated using a singular value decomposition of the matrix M

$$ M = \sum_{k=1}^{N} ({}^{H}\mathbf{AD}_k - {}^{H}\mathbf{AD})({}^{R}\mathbf{P}_k - {}^{R}\mathbf{P})^T = USV^T \tag{21} $$

$$ Q = VU^T. \tag{22} $$

The matrix Q is then converted into the unit quaternion ${}^{R}\hat{q}_H$. The translational ${}^{R}\mathbf{AO}$ part is obtained as

$$ {}^{R}\mathbf{AO} = \frac{1}{N}\sum_{k=1}^{N} ({}^{R}\mathbf{P}_k - Q\ {}^{H}\mathbf{AD}_k). \tag{23} $$

Parameters optimization. Parameters values error may be introduced during the initialization procedure and during the estimation of the human-robot transformation. The context of PbD enables to take advantages of the robot in order to optimize some parameters of the IHMT method. The parameters involved are the I2S orientations for each segment ${}^{Sin}\hat{q}_{in}\forall n$ simply noted here ${}^{Si}\hat{q}_i$ with $i \in [1,2,3]$; the original orientation of each sensor ${}^{H}\hat{q}_{Si0}$ with $i \in [1,2,3]$; the rotation ${}^{R}\hat{q}_H$ and the translation ${}^{R}\mathbf{AO}$. These errors mostly come from human parasitic motions. The term parasitic motion denotes all motions that come in addition to the desired action performed by the human and disturbing it. A non-exhaustive list can be given: torso or shoulder displacement, finger motion, skin and muscle motion resulting in sensor displacement with respect to the human segment, the arm not being horizontal nor straight during the measurement for $\mathbf{z}_H$ estimation, the rotation motion for $\mathbf{y}_H$ estimation being not exactly in the sagittal plan, a non-permanent contact between human fingertip and robot end-effector during

the human-robot transformation estimation procedure. In addition, the measurement of the segments lengths ${}^{1n}\mathbf{AB}$, ${}^{2n}\mathbf{BC}$, ${}^{3n}\mathbf{CD}$, directly made on the operator, can also include errors. Consequently, all the above-mentioned parameters are optimized. The optimization process is based on data recorded during the human-robot transformation estimation procedure. The robot end-effector positions ${}^{R}\hat{P}_k$ measured through robot encoders are used as reference. The human hand position with respect to the robot frame is computed from the estimation of the sensors orientation $q^{S10}\hat{q}_{S1k}$, ${}^{S20}\hat{q}_{S2k}$ and ${}^{S30}\hat{q}_{S3k}$ recorded simultaneously with the robot end-effector positions. The optimization is made by minimizing the following error function f:

$$\begin{aligned} f({}^{1n}\mathbf{AB}, {}^{2n}\mathbf{BC}, {}^{3n}\mathbf{CD}, {}^{S1}\hat{q}_1, {}^{S2}\hat{q}_2, {}^{S3}\hat{q}_3, {}^{H}\hat{q}_{S10}, {}^{H}\hat{q}_{S20}, {}^{H}\hat{q}_{S30}, {}^{H}\hat{q}_R, {}^{R}\mathbf{AO}) \\ = \sum_{k=1}^{N} \| {}^{R}\hat{P}_k - ({}^{R}\hat{q}_H \otimes {}^{H}\hat{AD}_k^* \otimes {}^{H}\hat{q}_R + {}^{R}\hat{AO}) \|^2 \end{aligned} \tag{24}$$

with

$${}^{H}\hat{AD}_k^* = {}^{H}\hat{q}_{1k}^* \otimes {}^{1k}\hat{AB} \otimes {}^{1k}\hat{q}_H^* + {}^{H}\hat{q}_{2k}^* \otimes {}^{2k}\hat{BC} \otimes {}^{2k}\hat{q}_H^* + {}^{H}\hat{q}_{3k}^* \otimes {}^{3k}\hat{CD} \otimes {}^{3k}\hat{q}_H^* \tag{25}$$

$${}^{H}\hat{q}_{1k}^* = {}^{H}\hat{q}_{S10} \otimes {}^{S10}\hat{q}_{S1k} \otimes {}^{S1}\hat{q}_1 \tag{26}$$

$${}^{H}\hat{q}_{2k}^* = {}^{H}\hat{q}_{S20} \otimes {}^{S20}\hat{q}_{S2k} \otimes {}^{S2}\hat{q}_2 \tag{27}$$

$${}^{H}\hat{q}_{3k}^* = {}^{H}\hat{q}_{S30} \otimes {}^{S30}\hat{q}_{S3k} \otimes {}^{S3}\hat{q}_3. \tag{28}$$

The optimization problem is solved using the optimize.minimize function from the SciPy library with the BFGS algorithm with a tolerance set to 10. The initial guess for the segment lengths ${}^{1n}\mathbf{AB}, {}^{2n}\mathbf{BC}$ and ${}^{3n}\mathbf{CD}$ are from a direct measurement on the operator arm. The values of the initial values of the I2S orientation ${}^{S1}\hat{q}_1, {}^{S2}\hat{q}_2$ and ${}^{S3}\hat{q}_3$ come from the initialization as well as the orientations $q^{S10}\hat{q}_{S1k}$, ${}^{S20}\hat{q}_{S2k}$ and ${}^{S30}\hat{q}_{S3k}$. Finally, ${}^{H}\hat{q}_R$ and ${}^{R}\mathbf{AO}$ initial guess are the values from the human-robot transformation estimation process described in the previous paragraph.

3. Experimental method and results

Three experiments are proposed to estimate error and validate the different elements of the method. First, the orientation estimation algorithm is compared to a reference and to other algorithms. The impact of the heading reset is highlighted as well as

the error of the complete algorithm. Secondly, the IHMT method is applied on a robot arm to verify the robustness of the method to the positioning of the sensors. Finally, the method is applied on a real human arm. Compared to the previous results, it enables to estimate the part of the error due to human parasitic motion.

3.1. Error and comparison on the estimated orientation

The proposed orientation estimation algorithm has been applied to the filtered data from Xsens MTw Awinda sensors [68]. It is considered that the filtered data from commercial sensors already present limited noise. A comparison is made with the orientation estimation algorithm from the company Xsens based on the Kalman filter and using magnetometer as well as with the Madgwick's algorithm [58], the Mahony's algorithm [52] and the Fourati's algorithm [69], without using a magnetometer. In order to validate the proposed method, three sensors are mounted on an ABB IRB 120 robot arm end-effector. The robot end-effector orientation ${}^{R}\hat{q}_{EEn}$, measured through encoders, is used as reference. The sensors are mounted in a way that initial sensor frame $Si0$ is aligned with the robot base frame R as well as the body-attached frame Sin and the end-effector frame EEn. The error ε, given in degree, is computed by

$$\varepsilon = \|{}^{R}\boldsymbol{\theta}\| = \|\log({}^{Sin}\hat{q}_{Si0} \otimes {}^{R}\hat{q}_{EEn})\| \tag{29}$$

In order to impose an orientation to the robot that reflects realistic human arm motion, a set of orientation values is created from the motion of the arm of two subjects. The two subjects wear one Xsens IMU sensor on each segment and they are asked to move their arm freely for 20 seconds with the only instruction to cover as much as possible the range of human arm motion. It can be mentioned that 68.1% of this motion is considered stationary regarding the criteria defined at the end of section 2.1. During the motion, the orientation of each sensor, estimated by the Xsens algorithm, is recorded to constitute a set of human realistic orientations. This set is played by the robot in two different ways: continuously then with a 1 second break between each orientation. Furthermore, this motion is repeated at different maximum robot end-effector velocities. This set of repeated trajectory constitutes a motion that lasts 3707 seconds so that the gyroscope bias has a significant impact on the motion estimation. Three measurements

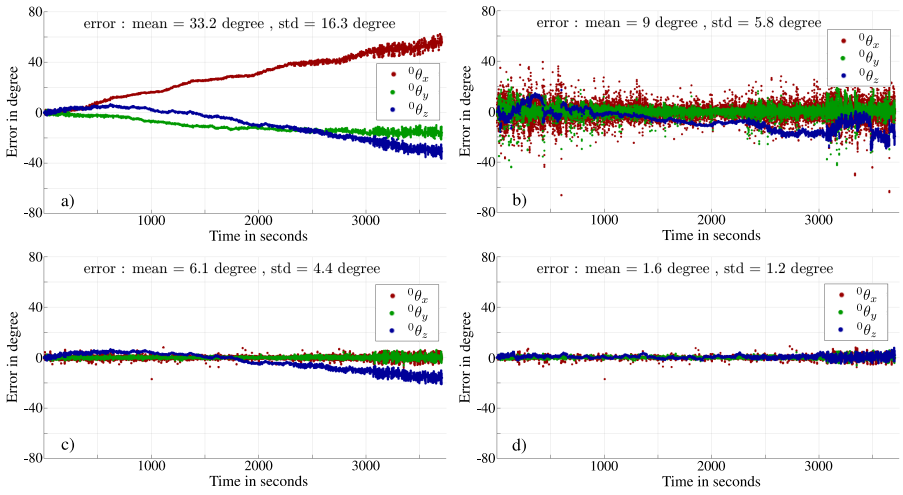

Figure 6: Rotation vector error ${}^0\boldsymbol{\theta}$ for the sensor 3 during measurement 3 from gyroscope integration to complete proposed algorithm: a) represents estimation made by gyroscope integration only, b) represents the orientation with stationary periods detected by the threshold on the accelerometer norm only, c) similar to b) but with a threshold on the jerk in addition for stationary periods detection, d) the complete algorithm.

of the described motion have been executed and the results for all algorithms are presented in Table 2. The proposed algorithm is more accurate than the other algorithms in this case. The influence of the different elements of the algorithm is shown in Figure 6, the complete algorithm providing the best performance. These encouraging results tend to confirm the validity of the hypothesis.

3.2. Evaluation of the initialization procedure

Experiment description. This section aims at validating the trajectory estimation method with respect to the inertial frame H as well as the robustness of the initialization procedure to the positioning of the sensors on each segment. Three Xsens MTw sensors have been mounted on an ABB IRB 120 robotic arm as shown in Figure 8. The support for sensors (upper right corner of Figure 8) enables to set the sensors to different orientations with respect to the segment frame. The robot has an anthropomorphic kinematics with one degree of freedom less than the human arm which enables to apply our method on this robotics arm. Axes 1 and 2 of the robot mimic the human

Measurement	Sensors	Xsens algorithm error	Mahony's algorithm error	Madgwick's algorithm error	Fourati's algorithm error	Proposed algorithm without Cj & $\boldsymbol{\omega}^{\text{reset}}$ error	Proposed algorithm with Cj without $\boldsymbol{\omega}^{\text{reset}}$ error	Proposed algorithm with Cj & $\boldsymbol{\omega}^{\text{reset}}$ error
1	1	34.8	23.3	24.8	24.8	6.8	25.5	2.5
	2	25.4	118.4	139.1	65.3	16.3	13.9	13.6
	3	12.5	38.4	154.9	33.3	6.8	34.2	2.0
2	1	19.9	21.9	30.3	30.4	6.9	29.8	2.3
	2	10.2	74.2	5.5	5.5	8.6	5.1	2.6
	3	37.7	116.3	110.5	87.4	23.0	14.3	4.0
3	1	26.6	107.5	97.0	81.4	31.6	7.5	2.1
	2	16.4	27.0	7.8	7.9	53.9	6.4	1.9
	3	8.4	50.9	47.8	6.2	9.0	6.1	1.6

Table 2: Mean error in degree on the orientation of the proposed algorithm with and without Cj (Cj is the criteria based on the jerk: $\| \frac{{}^{S0}\mathbf{a}_n - {}^{S0}\mathbf{a}_{n-1}}{\Delta t} \| < k_d$), and with and without $\boldsymbol{\omega}^{\text{reset}}$, the Xsens algorithm and three other IMU algorithms

shoulder with the center of the joint at the intersection of the axes. The human elbow is materialized by axis 3. Axes 4, 5 and 6 mimic the human wrist. So, the rotation of the human arm segment around the axis of the segment itself, has no equivalent in the robot kinematics. However, the arm model used in this work, composed of 3 spherical joints, is applicable to both human and robot kinematics, so that our method can be applied to the robot directly. The lengths of the robot segments are taken from the robot data sheet: $L_1 = 270$ mm, $L_2 = 310.0065$ mm, $L_3 = 72$ mm. The trajectory executed by the robot is composed of pure translations and rotations and a complex trajectory as can be seen in Figure 7. To build the complex trajectory, 6 points have been programmed and the robot goes through all the points with joint motion. For each measurement, the complete trajectory is repeated three times at different maximum velocities of the robot end-effector: 200 mm.s^{-1}, 100 mm.s^{-1} and 50 mm.s^{-1}. Fourteen measurements

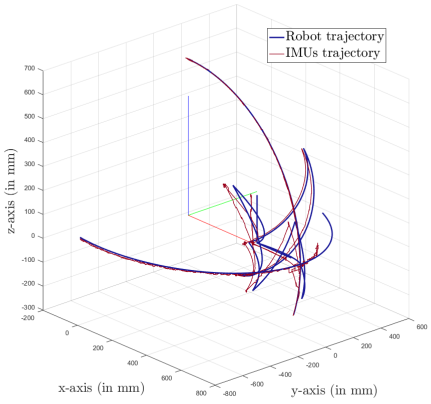

Figure 7: 3D trajectories measured by robot and IMUs (end-effector maximum velocity: 200 mm/s)

are made with different configurations of the sensors support. The absolute error is computed as $\varepsilon_t = \frac{1}{N}\sum_{k=1}^{N} \| {}^{H}\mathbf{AD}_k - {}^{R}\mathbf{P}_k \|$ with N the number of points. In this case, the frames R and H are aligned. No human-robot transformation estimation procedure is applied since no human is involved in this measurement. Consequently, parameters are not optimized. However, the robot is considered following accurately the required motion of the initialization.

Results. The results are presented in Table 3 and show an error comprised between 13.3 mm and 17.6 mm. These results are used as a basis for comparison in the next experiment.

Configuration	1	2	3	4	5	6	7
ε_t (in mm)	14.7	14.3	15.0	13.3	17.1	14.8	17.3
Configuration	8	9	10	11	12	13	14
ε_t (in mm)	15.2	13.8	14.1	16.6	17.6	14.7	15.7

Table 3: Mean error on the end-effector position for different configurations of sensors set up on a robotic arm

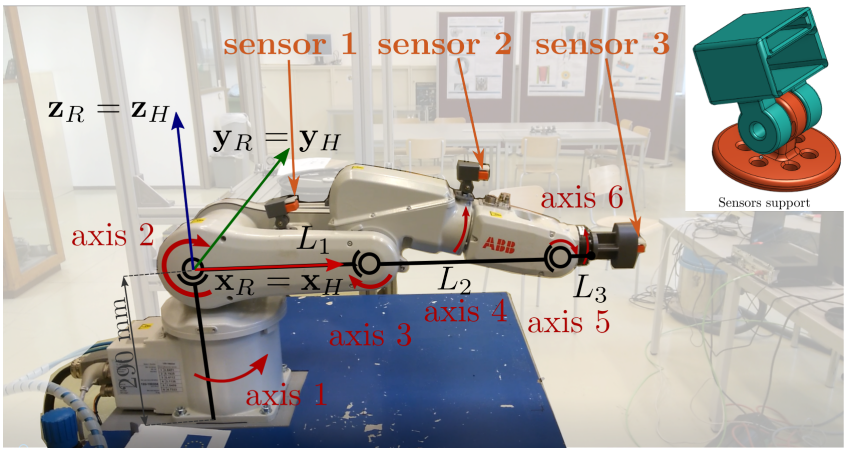

Figure 8: Set up for the experimental error measurement on the trajectory

3.3. Assessment of the method

This section presents an experimental application of the proposed method with a real human operator and a 7-DoF Sawyer collaborative robot from Rethink Robotics. The aim of this experiment is to evaluate the accuracy of the complete method i.e., the human hand trajectory with respect to the robot frame. Therefore, the robot is used to impose a trajectory to the operator (as in the human-robot transformation estimation procedure) and the trajectory measured by the robot encoders is used as the reference trajectory. The experiment is detailed below.

Setup. Two IMUs are set up on the arm and forearm with reflective metallic strips (see Fig. 9). The IMU for the hand is set in a gun-shaped tool. This tool includes a trigger button which can be used to go from step to step. The spherical tip of the gun fits in a receiver mounted at the robot end-effector to enforce the contact during the human-robot transformation estimation procedure and the recording of the human trajectory. In this way, the robot can impose a trajectory to the human during the recording. The trajectory recorded through the robot encoders is used as reference. The measured segment dimensions of the subject are, in millimeters, ${}^{1n}\mathbf{AB}_n = [330\ 0\ 0]^T$, ${}^{2n}\mathbf{BC}_n = [277\ 0\ 0]^T$, ${}^{3n}\mathbf{CD}_n = [280\ -20\ 110]^T\ \ \forall n$. ${}^{3n}\mathbf{CD}_n$ is not aligned with the **x**-axis of the segment due to the gun-shaped tool. The minimization process is conducted

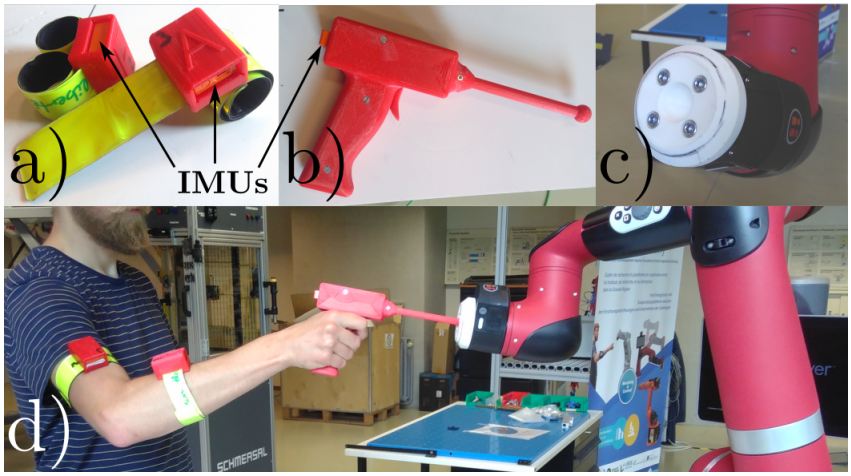

Figure 9: Setup for the application of the proposed method: a) IMUs set on the arm and forearm, b) gun-shaped tool with the trigger button, c) end-effector hole to receive the tip of the tool, d) global view of the setup

by the optimize.minimize function from the SciPy library with the BFGS algorithm as explained in the paragraph *Parameters optimization* in the subsection *2.2 Hand trajectory estimation*. Different trajectories are executed by a unique operator (see Fig. 10). The error ε_t is the mean distance between the estimated point from IMU measurement ${}^{R}\mathbf{AD}_k$ and the reference one measured by the robot encoders ${}^{R}\mathbf{P}_k$, computed as $\varepsilon_t = \frac{1}{N}\sum_{k=1}^{N} \|{}^{R}\mathbf{P}_k - {}^{R}\mathbf{AD}_k\|$ with N the number of points. The results are exposed in Table 4.

Results and discussion. First, the results presented in Table 4 show the positive impact of the optimization. The difference between non-optimized and optimized values of each parameter is computed for all trials. Table 5 gives the maximum and the mini-

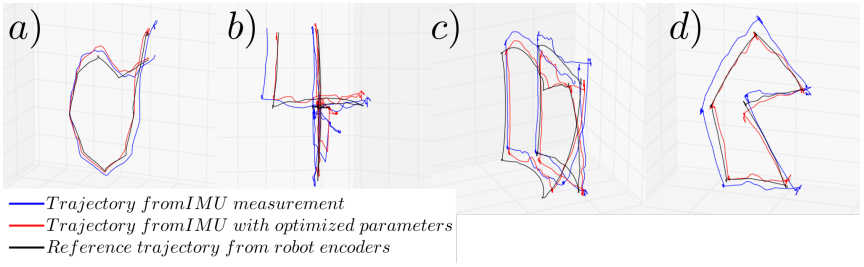

Figure 10: Trajectory imposed by the robot: a) “Circle” trajectory, b) “Cross” trajectory, c) “Cube” trajectory, d) “Hexagon” trajectory

Measurement	Time (in s)	non-optimized parameters		optimized parameters	
		Error (in mm)	standard deviation (in mm)	Error (in mm)	standard deviation (in mm)
Circle 1	8.55	52.0	14.7	32.9	20.5
Circle 2	7.91	53.8	12.7	28.8	10.8
Circle 3	8.25	50.1	19.7	29.4	12.8
Cross 1	27.99	55.5	32.7	39.9	26.0
Cross 2	27.71	47.2	28.4	42.8	20.1
Cross 3	27.08	77.0	35.0	61.8	27.4
Cube 1	44.24	85.8	33.5	45.0	13.4
Cube 2	39.19	96.2	53.7	50.4	20.5
Cube 3	39.07	83.8	43.4	39.8	17.7
Hexagon 1	28.47	55.4	16.4	28.5	16.7
Hexagon 2	27.77	68.5	26.5	40.9	20.5
Hexagon 3	27.09	70.7	26.4	52.8	22.1

Table 4: Human arm trajectory in robot base frame error

mum of these differences. The differences are low, meaning the parameters conserve a physically realistic value.

Secondly, the error is comprised between 28.5 mm and 61.8 mm. Let us recall that

Parameters	Maximum difference	Minimum difference
${}^{1n}\mathbf{AB}$	0.53 mm	0.012 mm
${}^{2n}\mathbf{BC}$	0.44 mm	0.012 mm
${}^{3n}\mathbf{CD}$	0.29 mm	0.003 mm
${}^{S1}\hat{q}_1$	21.8 °	13.0 °
${}^{S2}\hat{q}_2$	32.7 °	20.0 °
${}^{S3}\hat{q}_3$	32.9 °	20.3 °
${}^{H}\hat{q}_{S10}$	27.1 °	8.6 °
${}^{H}\hat{q}_{S20}$	23.4 °	7.8 °
${}^{H}\hat{q}_{S30}$	33.3 °	6.2 °
${}^{H}\hat{q}_{R}$	23.6 °	3.2 °
${}^{R}\mathbf{AO}$	1.2 mm	0.015 mm

Table 5: Differents of values before and after optimization

error on the trajectory measured in the previous subsection on a robot is comprised between 13.3 mm and 17.6 mm. This difference may come from several factors associated with the human anatomy, the behavior of the operator and the limits of the proposed method, as discussed in the following:

- The transformation from the human frame to the robot frame was not necessary in the previous experiment. This step may introduce some error.
- Several parasitic motions affect the measurement such as: the torso and shoulder displacement; the motion of the gun with respect to the palm of the hand; the motion of the sensors with respect to the segment and forearm due to soft tissues displacements and strapping system displacement; or the shakiness of the human motion.
- As shown in [70] and [71] the shoulder center of rotation is not unique and depends on the position of the arm. The model of the shoulder in this work does not reflect this complexity.

- Some error may also be attributed to unmet assumptions of the initialization process. In particular, the arm might not be perfectly horizontal or stretched and the rotation might be disturbed. The optimization step catches up only a part of this error.

- The contact between the tip of the gun and the robot end-effector used during the human-robot transformation estimation procedure and the recording of the trajectory is not strictly guaranteed, especially if the robot moves back. Regarding the human-robot transformation estimation, this source of error is inherent to the method. Regarding the measurement, this source of error is inherent to the experimental setup. However, the measurements with obvious missing contact are discarded so that this source of error has a negligible impact compared to the other sources of error mentioned above.

Despite the listed sources of error, the proposed method gives a reliable estimation of the trajectory. Our results can be put in perspective with the survey of Filippeschi et al. [22]. In this work, the trajectory of the wrist for different elementary arm motion (flexion/extension, pro-and supination ...) is estimated with 5 different IHMT methods. The methods are based on complementary filter, Kalman filter, extended Kalman filter or unscented Kalman filter. All methods are based on MIMU sensors but the magnetometer is not always exploited. An optical motion capture system measures human arm motion which is used as reference. The error is computed as the mean of the distance between inertial-based estimation and the reference. The results over trials and elementary motion can be summarized in Table 6. Our method presents results between 28.5 mm and 61.8 mm which are comparable to the best results presented in [22]. In addition, our results represent to the human hand trajectory with respect to the robot frame, which fits the expectation of a PbD application. In order to obtain this information based on the methods given in [22], additional disturbances caused by the hand segment tracking and the human-robot transformation, would alter the quality of the estimation. Table 4 shows that the optimization step is a key element to reach a competitive level of accuracy. Thus, our IHMT method reach a good level of accuracy and fulfill the constraints of a PbD application.

Methods	1	2	3-Pure	3-Perfect	4	5
Maximum error (mm)	108.9	243.8	156.0	272.2	98.3	214.4
Minimum error (mm)	23.6	60.9	27.8	36.5	72.3	44.8

Table 6: Mean error for different method from [22]

Conclusion

This work proposes an intuitive and easy-to-use method for human hand trajectory tracking based on IMUs for robotics applications. This method is suitable for demonstration acquisition in a robot PbD process.

Three IMUs sensors are mounted respectively on the hand, forearm and arm. The trajectory is computed from the orientation of each segment estimated from IMU sensors and the lengths of each segment of the arm. An initialization step is necessary to identify the I2S orientation as well as the human reference frame. This step consists of a rotation around the shoulder of the arm outstretched, defining **y**-axis through gyroscope measurement and then a horizontal static pose, defining **z**-axis through accelerometer measurement. It is shown that this procedure is robust to arbitrary positioning and orientation of the sensors on the arm.

This initialization is followed by a human-robot transformation estimation procedure to estimate the transformation from the human reference frame to the robot base frame. During this step, the robot imposes a trajectory to the human by contact between the human fingertip and the robot end-effector. The recorded data are also used in an optimization process of the following parameters: the segment vectors with respect to their segment frame; the I2S orientations; the initial sensor orientation with respect to the reference frame and the human-robot transformation.

The main challenge when using IMU is to estimate their orientation. A new drift-compensated algorithm is proposed, tested and compared to four other algorithms. This algorithm relies on gyroscope data integration and gravity vector observation method. The main contribution consists in exploiting a human motion property to compensate the drift around the gravity direction. For a task demonstration, it is assumed that the

operator naturally execute motions such that the sensors pass by their original heading (with different inclinations) several times during the task. This is exploited to reset the drift each time this situation is encountered. This algorithm, tested for a long and realistic human motion on commercial sensors, gives encouraging results. The strong assumptions made on human motions to apply IMU heading reset seem therefore validated in a context of robot programming by demonstration.

Finally, the complete method has been implemented on a Sawyer robot. Different trajectories are imposed to the human by the robot and directly recorded by its encoders to be used as reference. For the movement of the human arm motion, the results show a mean error comprised between 28.5 mm and 61.8 mm whereas the results of the method applied to a robot gives an error between 13.3 mm and 17.6 mm. It reveals that the human arm motion induces several disturbances lowering the accuracy of the method. Improving the accuracy might be possible, for instance by using a more detailed human arm model and by measuring the human parasitic motion. However, in the case of a human demonstration for PbD, a high level of accuracy on the complete trajectory is not necessary. For instance, in a pick and place application, precision is mainly required at the pick and place positions so that local improvement of the trajectory might be enough.

As a future work, this method could be tested in a complete PbD process. In such an application, a demonstration might require information about the environment such as that the object position in a pick and place task. In that case, managing the information on the human trajectory and the environment could represent another challenge. Furthermore, in human interactions, non-verbal symbolic gestures are often used. As IMUs have been largely used in the human gesture recognition, extracting, identifying and adding symbolic human gesture to a demonstration could be investigated.

Acknowledgment

This work was supported by the Interreg V program of the Greater Region within the Robotix Academy project.

References

[1] A. Billard, S. Calinon, R. Dillmann, S. Schaal, Robot Programing by Demonstration, in: Springer Handbook of Robotics, Springer, 2008, pp. 1371–1394. doi:10.1007/978-3-540-30301-5_60.

[2] M. Ehrenmann, R. Zöllner, O. Rogalla, R. Dillmann, Programming service tasks in household environments by human demonstration, Proceedings of the IEEE International Workshop on Robot and Human Interactive Communication (2002) 460–467.

[3] B. D. Argall, S. Chernova, M. Veloso, B. Browning, A survey of robot learning from demonstration, Robotics and Autonomous Systems 57 (5) (2009) 469–483. doi:10.1016/j.robot.2008.10.024.

[4] P. Abbeel, Andrew Y. Ng, Apprenticeship learning via inverse reinforcement learning, Proceedings of the twenty-first international conference on Machine learning (2004). doi:10.1145/1015330.1015430.

[5] C. Breazeal, M. Berlin, A. Brooks, J. Gray, A. L. Thomaz, Using perspective taking to learn from ambiguous demonstrations, Robotics and Autonomous Systems 54 (5) (2006) 385–393. doi:10.1016/j.robot.2006.02.004.

[6] S. Chernova, M. Veloso, Multi-thresholded approach to demonstration selection for interactive robot learning, Proceedings of the 3rd International Conference on Human-Robot Interaction (2008) 225–232doi:10.1145/1349822.1349852.

[7] A. Vakanski, I. Mantegh, A. Irish, F. Janabi-Sharifi, Trajectory Learning for Robot Programming by Demonstration Using Hidden Markov Model and Dynamic Time Warping, in: IEEE Transactions on Systems, Man, and Cybernetics, Part B (Cybernetics), Vol. 42, 2012, pp. 1039–1052. doi:10.1109/TSMCB.2012.2185694.

[8] M. Ogino, H. Toichi, Y. Yoshikawa, M. Asada, Interaction rule learning with a human partner based on an imitation faculty with a simple visuo-motor mapping,

Robotics and Autonomous Systems 54 (5) (2006) 414–418. doi:10.1016/j.robot.2006.01.005.

[9] U. Nehmzow, O. Akanyeti, C. Weinrich, T. Kyriacou, S. A. Billings, Robot programming by demonstration through system identification, Proceedings of the IEEE International Conference on Intelligent Robots and Systems (2007) 801–806.

[10] S. Calinon, A. Billard, Teaching a humanoid robot to recognize and reproduce social cues, Proceedings of the 15th IEEE International Symposium on Robot and Human Interactive Communication (2006) 346–351doi:10.1109/ROMAN.2006.314458.

[11] K. Ogawara, J. Takamatsu, H. Kimura, K. Ikeuchi, Generation of a task model by integrating multiple observations of human demonstrations, Proceedings of the IEEE International Conference on Robotics and Automation (Cat. No.02CH37292) (2002) 1545–1550doi:10.1109/ROBOT.2002.1014763.

[12] A. Ijspeert, J. Nakanishi, S. Schaal, Trajectory formation for imitation with nonlinear dynamical systems, Proceedings of the IEEE/RSJ International Conference on Intelligent Robots and Systems. Expanding the Societal Role of Robotics in the Next Millennium (Cat. No.01CH37180) (2001). doi:10.1109/IROS.2001.976259.

[13] J. Li, J. Wang, S. Wang, C. Yang, Human–robot skill transmission for mobile robot via learning by demonstration, Neural Computing and Applications 0123456789 (2021). doi:10.1007/s00521-021-06449-x.
URL https://doi.org/10.1007/s00521-021-06449-x

[14] Z. Chen, J. Li, S. Wang, J. Wang, L. Ma, Flexible gait transition for six wheel-legged robot with unstructured terrains, Robotics and Autonomous Systems 150 (2022) 103989. doi:10.1016/j.robot.2021.103989.
URL https://doi.org/10.1016/j.robot.2021.103989

[15] J. Kaiser, S. Melbaum, J. C. V. Tieck, A. Roennau, M. V. Butz, R. Dillmann, Learning to Reproduce Visually Similar Movements by Minimizing Event-Based Prediction Error, Proceedings of the IEEE RAS and EMBS International Conference on Biomedical Robotics and Biomechatronics 2018-August (2018) 260–267. doi:10.1109/BIOROB.2018.8487959.

[16] A. Kendon, Gesture: Visible Action as Utterance, Cambridge University Press, 2004.

[17] J. A. Mosher, The essentials of effective gesture, for students of public speaking, New York, The Macmillan company, 1916.

[18] M. Kyrarini, M. A. Haseeb, D. Ristić-Durrant, A. Gräser, Robot Learning of Object Manipulation Task Actions From Human Demonstrations, Facta Universitatis, Series: Mechanical Engineering 15 (2) (2017) 217.

[19] M. Johnson, Y. Demiris, Abstraction in recognition to solve the correspondence problem for robot imitation, Taros (2004) 63–70.
URL http://cswww.essex.ac.uk/technical-reports/2004/csm415/Johnson_Demiris.pdf

[20] M. Ferreira, P. Costa, L. Rocha, A. Moreira, Stereo-based real-time 6-Dof work tool tracking for robot programing by demonstraiton.pdf, The International Journal of Advanced Manufacturing Technology (2014).

[21] M. Field, D. Stirling, F. Naghdy, Z. Pan, Motion capture in robotics review, Proceedings of the IEEE International Conference on Control and Automation (2009) 1697–1702.

[22] A. Filippeschi, N. Schmitz, M. Miezal, G. Bleser, E. Ruffaldi, D. Stricker, Survey of motion tracking methods based on inertial sensors: A focus on upper limb human motion, Sensors (Switzerland) 17 (6) (2017) 1257. doi:10.3390/s17061257.

[23] T. Grisbrook, C. Imms, C. P. Walmsley, A. C. Campbell, C. Elliott, S. A. Williams, Measurement of upper limb range of motion using wearable sen-

sors: A systematic review, Sports Medicine - Open 4 (1) (2018) 53–75. doi:10.1186/s40798-018-0167-7.

[24] M. T. Wolf, C. Assad, M. T. Vernacchia, J. Fromm, H. L. Jethani, Gesture-based robot control with variable autonomy from the JPL BioSleeve, Proceedings of the IEEE International Conference on Robotics and Automation (2013) 1160–1165doi:10.1109/ICRA.2013.6630718.

[25] A. Ijspeert, J. Nakanishi, S. Schaal, Nonlinear dynamical systems for imitation with humanoid robots (December) (2003) 1398–1403.

[26] S. Calinon, A. Billard, Incremental learning of gestures by imitation in a humanoid robot, Proceeding of the ACM/IEEE international conference on Human-robot interaction - HRI '07 (2007) 255.

[27] V. H. Pinto, A. Amorim, L. Rocha, A. P. Moreira, Enhanced performance real-time industrial robot programming by demonstration using stereoscopic vision and an IMU sensor, IEEE International Conference on Autonomous Robot Systems and Competitions (2020). doi:10.1109/ICARSC49921.2020.9096200.

[28] W.-Y. Go, J.-H. Kim, Wireless Remote Control of Robot Dual Arms and Hands Using Inertial Measurement Units, in: Proc. International Conference on Robot Intelligence Technology and Applications (RiTA), Beijing, 2014, pp. 759–768.

[29] X. Chen, Human Motion Analysis with Wearable Inertial Sensors, IEEE Sensors Journal 16 (22) (2016) 7821–7834. doi:10.1109/JSEN.2016.2609392.

[30] M. Miezal, B. Taetz, G. Bleser, On inertial body tracking in the presence of model calibration errors, Sensors (Switzerland) 16 (7) (2016) 1132. doi:10.3390/s16071132.

[31] P. Cheng, B. Oelmann, Joint-angle measurement using accelerometers and gyroscopes - A survey, IEEE Transactions on Instrumentation and Measurement 59 (2) (2010) 404–414. doi:10.1109/TIM.2009.2024367.

[32] A. Gallagher, Y. Matsuoka, Wei-Tech Ang, An efficient real-time human posture tracking algorithm using low-cost inertial and magnetic sensors, Proceedings of the IEEE/RSJ International Conference on Intelligent Robots and Systems (IROS) (2004). doi:10.1109/IROS.2004.1389860.

[33] H. J. Luinge, P. H. Veltink, Measuring orientation of human body segments using miniature gyroscopes and accelerometers, Medical and biological engineering and computing 43 (2) (2005) 273 – 282. doi:10.1007/bf02345966.

[34] Y. Xiaoping, E. R. Bachmann, Design, implementation, and experimental results of a quaternion-based kalman filter for human body motion tracking, IEEE Transactions on Robotics 22 (6) (2006) 1216–1227. doi:10.1109/TRO.2006.886270.

[35] Y. Tian, J. Tan, A fast adaptive-gain orientation filter of inertial/magnetic data for human motion tracking in free-living environments, The Journal of Navigation 71 (6) (2018) 1478 – 1491. doi:10.1017/S0373463318000231.

[36] H. Zhou, H. Hu, Reducing drifts in the inertial measurements of wrist and elbow positions, IEEE Transactions on Instrumentation and Measurement 59 (3) (2010) 575–585. doi:10.1109/TIM.2009.2025065.

[37] L. Peppoloni, A. Filippeschi, E. Ruffaldi, C. A. Avizzano, A novel 7 degrees of freedom model for upper limb kinematic reconstruction based on wearable sensors, Proceedings of the IEEE 11th International Symposium on Intelligent Systems and Informatics (SISY) (2013). doi:10.1109/SISY.2013.6662551.

[38] E. Palermo, S. Rossi, F. Marini, F. Patanè, P. Cappa, Experimental evaluation of accuracy and repeatability of a novel body-to-sensor calibration procedure for inertial sensor-based gait analysis, Measurement: Journal of the International Measurement Confederation 52 (1) (2014) 145–155. doi:10.1016/j.measurement.2014.03.004.

[39] X. Robert-lachaine, H. Mecheri, C. Larue, S. Bellefeuille, Single pose calibration

with inertial measurement units, Gait and Posture 54 (2017) 80–86. doi:10.1016/j.gaitpost.2017.02.029.

[40] W. De Vries, H. E. Veeger, A. G. Cutti, C. Baten, F. C. van der Helm, Functionally interpretable local coordinate systems for the upper extremity using inertial and magnetic measurement systems, Journal of Biomechanics 43 (10) (2010) 1983–1988. doi:10.1016/j.jbiomech.2010.03.007.

[41] M. Zabat, A. Ababou, N. Ababou, R. Dumas, IMU-based sensor-to-segment multiple calibration for upper limb joint angle measurement—a proof of concept, Medical and Biological Engineering and Computing 57 (2019) 2449–2460. doi:10.1007/s11517-019-02033-7.

[42] C. Jiang, M. Fahad, Y. Guo, J. Yang, Y. Chen, Robot-assisted human indoor localization using the Kinect sensor and smartphones, Proceedings of the IEEE International Conference on Intelligent Robots and Systems (2014).

[43] S. S. Ghidary, Y. Nakata, T. Takamori, M. Hattori, Localization and approaching to the human by mobile home robot, in: Proceedings of the IEEE International Workshop on Robot and Human Interactive Communication, 2000.

[44] M. Faessler, E. Mueggler, K. Schwabe, D. Scaramuzza, A monocular pose estimation system based on infrared LEDs, Proceedings of the IEEE International Conference on Robotics and Automation (ICRA) (2014). doi:10.1109/ICRA.2014.6906962.

[45] B. Gromov, L. M. Gambardella, A. Giusti, Robot Identification and Localization with Pointing Gestures, in: Proceedings of the IEEE/RSJ International Conference on Intelligent Robots and Systems (IROS), 2018, pp. 3921–3928. doi:10.1109/IROS.2018.8594174.

[46] D. Roetenberg, L. Henk, V. Peter, Inertial and magnetic sensing of human movement near ferromagnetic materials, in: Proceedings of the second IEEE and ACM International Symposium on Mixed and Augmented Reality, 2003. doi:10.1109/ISMAR.2003.1240714.

[47] G. Ligorio, A. M. Sabatini, Dealing with magnetic disturbances in human motion capture: A survey of techniques, Micromachines 7 (3) (2016) 43. doi:10.3390/mi7030043.

[48] W. De Vries, H. Veeger, C. Baten, F. C. van der Helm, Magnetic distortion in motion labs, implications for validating inertial magnetic sensors, Gait and Posture 29 (4) (2009) 535–541. doi:10.1016/j.gaitpost.2008.12.004.

[49] S. Zihajehzadeh, E. J. Park, A Novel Biomechanical Model-Aided IMU/UWB Fusion for Magnetometer-Free Lower Body Motion Capture, IEEE Transactions on Systems, Man, and Cybernetics: Systems 47 (6) (2017) 927–938. doi:10.1109/TSMC.2016.2521823.

[50] M. Kok, J. D. Hol, T. B. Schön, Using inertial sensors for position and orientation estimation, Foundations and Trends® in Signal Processing 11 (1-2) (2017) 1–153. doi:10.1561/2000000094.

[51] I. H. López-nava, A. Muñoz-Meléndez, Wearable inertial sensors for human motion analysis : A review, IEEE Sensors Journal 16 (22) (2016) 7821–7834. doi:10.1109/JSEN.2016.2609392.

[52] R. Mahony, T. Hamel, J.-M. Pflimlin, Non-linear complementary filters on the special orthogonal group, IEEE Transactions on Automatic Control 53 (5) (2008) 1203–1218. doi:10.1109/TAC.2008.923738.

[53] H. Fourati, Heterogeneous data fusion algorithm for pedestrian navigation via foot-mounted inertial measurement unit and complementary filter, IEEE Transactions on Instrumentation and Measurement 64 (1) (2015) 221.229. doi:10.1109/TIM.2014.2335912.

[54] M. Euston, P. Coote, R. Mahony, J. Kim, T. Hamel, A complementary filter for attitude estimation of a fixed-wing UAV, Proceedings of the IEEE/RSJ International Conference on Intelligent Robots and Systems (2008) 340–345doi:10.1109/IROS.2008.4650766.

[55] A. Kim, M. Golnaraghi, A quaternion-based orientation estimation algorithm using an inertial measurement unit, Proceedings of the Position Location and Navigation Symposium (2004). doi:10.1109/PLANS.2004.1309003.

[56] D. Choukroun, I. Y. Bar-Itzhack, Y. Oshman, Novel quaternion Kalman filter, IEEE Transactions on Aerospace and Electronic Systems 42 (1) (2006) 174–190. doi:10.1109/TAES.2006.1603413.

[57] A. Barrau, S. Bonnabel, Invariant Kalman Filtering, Annual Review of Control, Robotics, and Autonomous Systems 1 (2018) 237–257. doi:10.1146/annurev-control-060117-105010.

[58] S. Madgwick, An efficient orientation filter for inertial and inertial/magnetic sensor arrays, Technical Report X-io (2010).

[59] H. P. Brückner, C. Spindeldreier, H. Blume, E. Schoonderwaldt, E. Altenmüller, Evaluation of inertial sensor fusion algorithms in grasping tasks using real input data: Comparison of computational costs and root mean square error, Proceedings of the Ninth International Conference on Wearable and Implantable Body Sensor Networks (2012). doi:10.1109/BSN.2012.9.

[60] W. Hu, E. Charry, M. Umer, A. Ronchi, S. Taylor, An inertial sensor system for measurements of tibia angle with applications to knee valgus/varus detection, Proceedings of the IEEE Ninth International Conference on Intelligent Sensors, Sensor Networks and Information Processing (ISSNIP) (2014). doi:10.1109/ISSNIP.2014.6827603.

[61] A. Bandini, J. Zariffa, Analysis of the hands in egocentric vision: A survey, IEEE Transactions on Pattern Analysis and Machine Intelligence (2020) 1–1arXiv:1912.10867, doi:10.1109/tpami.2020.2986648.

[62] I. Rodriguez, M. Peinado, R. Boulic, D. Meziat, Bringing the human arm reachable space to a virtual environment for its analysis, Proceedings - IEEE International Conference on Multimedia and Expo 1 (August) (2003) 229–232. doi:10.1109/ICME.2003.1220896.

[63] J. Clément, M. Raison, D. M. Rouleau, Reproducibility analysis of upper limbs reachable workspace, and effects of acquisition protocol, sex and hand dominancy, Journal of Biomechanics 68 (2018) 58–64. doi:10.1016/j.jbiomech.2017.12.010.

[64] T. Beravs, J. Podobnik, M. Munih, Three-axial accelerometer calibration using Kalman filter covariance matrix for online estimation of optimal sensor orientation, IEEE Transactions on Instrumentation and Measurement 61 (9) (2012) 2501–20511. doi:10.1109/TIM.2012.2187360.

[65] D. Tedaldi, A. Pretto, E. Menegatti, A Robust and Easy to Implement Method for IMU Calibration without External Equipments, in: Proceedings of the IEEE International Conference on Robotics and Automation (ICRA), 2014. doi:10.1109/ICRA.2014.6907297.

[66] M. S. Andrle, J. L. Crassidis, Geometric integration of quaternions, Journal of Guidance, Control, and Dynamics 36 (6) (2013) 1762–1772. doi:10.2514/1.58558.

[67] K. S. Arun, T. S. Huang, S. D. Blostein, Least-squares fitting of two 3-d point sets, IEEE Transactions on Pattern Analysis and Machine Intelligence PAMI-9 (5) (1987) 698–700. doi:10.1109/TPAMI.1987.4767965.

[68] M. Paulich, M. Schepers, N. Rudigkeit, G. Bellusci, Xsens MTw Awinda: Miniature wireless inertial-magnetic motion tracker for highly accurate 3D kinematic applications, Whitepaper (2013).

[69] H. Fourati, N. Manamanni, L. Afilal, Y. Handrich, Complementary observer for body segments motion capturing by inertial and magnetic sensors, IEEE/ASME Transactions on Mechatronics 19 (1) (2014) 149–157. doi:10.1109/TMECH.2012.2225151.

[70] C. Amabile, A. M. J. Bull, A. E. Kedgley, The centre of rotation of the shoulder complex and the effect of normalisation, Journal of Biomechanics 49 (9) (2016) 1938–1943. doi:10.1016/j.jbiomech.2016.03.035.

[71] A. C. Campbell, J. A. Alderson, B. C. Elliott, D. G. Lloyd, Effects of different technical coordinate system definitions on the three dimensional representation of the glenohumeral joint centre, Medical and Biological Engineering and Computing 47 (5) (2009) 543–550. doi:10.1007/s11517-009-0467-7.